

Glass Europe Vol. 3 (2025) 203-219

https://doi.org/10.52825/glass-europe.v3i.2742

© Authors. This work is licensed under a Creative Commons Attribution 4.0 International License

Submitted: 12 Mar. 2025 | Accepted: 25 Sep. 2025 | Published: 15 Oct. 2025

Precipitation Kinetics of Nucleating Agents in LAS Glass-Ceramics by High Temperature Raman Spectroscopy

Jessica Streichert¹, Stefanie Meyer¹, Alessio Zandona¹, Danilo Di Genova², and Joachim Deubener^{1,*}

¹Clausthal University of Technology, Institute of Non-Metallic Materials, Zehntnerstr. 2a, D–38678 Clausthal-Zellerfeld, Germany

²Institute of Science, Technology and Sustainability for Ceramics (ISSMC) of the National Research Council (CNR), Via Granarolo 64, I–48018, Faenza, RA, Italy

*Correspondence: Joachim Deubener, joachim.deubener@tu-clausthal.de

Abstract. The precipitation kinetics of nucleating agents in technical lithium aluminosilicate (LAS) glass-ceramics is challenging to determine in laboratory practice due to the low content of about 3 wt%. Therefore, isothermal heat treatment series in the temperature range 750–820 °C with simultaneous recording of Raman spectra were carried out, which revealed a two-fold crystallisation process. In the first stage, an increase in oxygen coordination of Ti⁴⁺ from 4 and 5 to 6 is indicated, which was assigned to a liquid-liquid phase separation, while in the second stage ordering of the short range led to crystallisation of TiO₂(B) and anatase in the demixed domains. Using a sectional JMAK analysis of the temporally decoupled process, a stationary nucleation mechanism with no detectable growth is proposed for the first stage, while the second stage led to almost no change in volume fraction over time.

Keywords: Nucleation Agents, LAS Glass-Ceramics, Precipitation Kinetics

1. Introduction

Lithium aluminium silicate (LAS) glass ceramics have been thoroughly examined, as there is a wealth of technical products with low thermal expansion that are manufactured from this composition [1], [2], [3]. For the LAS system, the classical production route predominates, which can be divided into hot forming of the melt and the subsequent ceramisation of the formed glass by heat treatment [4]. The latter leads to the crystallisation of functional phases with anisotropic negative thermal expansion (quartz solid solutions (Qz-ss) and keatite solid solutions (Kea-ss) [5]) in the volume of the glass; because of the residual glass phase with positive thermal expansion, the overall thermal expansion of the crystallised material balances to zero. In order to trigger the crystallisation of Qz-ss inside the glass, so-called nucleating agents (or seed formers) are added to the batch, whose task is to provide an active site for heterogeneous nucleation of Qz-ss by early precipitation during ceramisation. As the amount of nucleating agents in the batch is relatively low (usually about 3% by weight) and the size of the crystallites formed from them during ceramisation rarely exceeds 4 nm [6], it is technically challenging to determine their precipitation kinetics using conventional laboratory analytics such as X-ray diffraction alone. Thus, Kleebusch et al. [7] combined XRD analysis with transmission electron microscopy (TEM) to study the precipitation of Zr_{1-x}Ti_{1+x}O₄ in a LAS glass using the nucleating agents TiO₂ and ZrO₂ in concentrations of 2.1 and 0.9 mol %, respectively. In particular, TEM has been used for advanced analyses to directly reveal the formation and nature of the seed forming crystals at the nanoscale [6], [8], [9].

At the macroscale, the properties of the glass that change due to the precipitation of seed former crystallites, such as optical transmittance [10], glass transition temperature and viscosity [11], were determined to provide an indication of the kinetics of this process. Recently, the relationship between the rheological and calorimetric response of glass has been of particular interest, as nanocrystallites play an important role not only in technical glass-ceramics, but also in natural melts where they are expected to drive explosive volcanism [12], [13], [14], [15]. Thus, the changes associated with the precipitation of the nanocrystallites can be indirectly determined, since the effective viscosity is fed by the steric effects of the suspended rigid particles and the changing chemical composition of the liquid matrix, while the caloric glass transition temperature only reflects the relaxation of the liquid matrix. In this context, it became clear that Raman spectroscopy is capable of detecting the short-range-order structure around seed formers cations during ceramisation conditions with high sensitivity [11], which is also confirmed by former studies of Alekseeva et al. [16], [17], [18], [19], [20], [21], Champagnon et al. [22], Zhilin et al., [23], Sprengard [24] and Gabel et al. [25] on the early phase transformations in LAS glasses seeded by TiO₂ and ZrO₂. In TiO₂-nucleated LAS glasses, it was found that the polymorph TiO₂(B), whose structural arrangement is more similar to the glass structure, is initially formed and subsequently transforms into anatase with increasing ceramisation time or temperature according to the Ostwald step rule [26]. It was also shown that the precipitation is preceded by a change in the oxygen coordination of the Ti⁴⁺ cations, which was related to demixing at the nanoscale [6], [9], [11], [16], [17], [20], [21], [24], [25]. However, there are only a few kinetic analyses of these processes, and further research is needed to provide a more comprehensive overview of the subject. Sprengard [24] found an Avrami coefficient of 1 ± 0.15 in a 1Li₂O·1Al₂O₃·6SiO₂ glass with 4 mol% TiO₂ for the change of the Ti⁴⁺ coordination from tetrahedral to octahedral (demixing) using data of deconvoluted Raman spectra from stopped ceramisation samples with molar concentration factors for the fraction at around 900 cm⁻¹. Donfeu Tchana et al. [10] determined an Avrami coefficient of 1.3, which results from the change in optical extinction at room temperature after stopping the ceramisation for different times, while Höche et al. [6] used a combination of transmission electron microscopy with Xray absorption near-edge structure spectroscopy to determine an Avrami coefficient of 1 for the formation of liquid-liquid phase separation droplets preceding the crystallisation of the seed former. The experiments in the latter two studies were also carried out at room temperature with samples in which the ceramisation process was stopped, and thus no experimental in situ data are yet available.

Against this background, the isothermal precipitation of the nucleating agent in LAS glass is investigated in situ using Raman spectroscopy and a heating stage. In order to be able to draw conclusions about the mechanism involved, the precipitation processes are simulated on the basis of a dual Johnson-Mehl-Avrami-Kolmogorov (JMAK) equation to enable a continuous description of the process.

2. Experimental

2.1 Glass preparation

A glass of lithium aluminosilicate (LAS) composition close to the stoichiometry $0.5\text{Li}_2\text{O} \cdot 0.25(\text{Zn},\text{Mg})\text{O} \cdot 1\text{Al}_2\text{O}_3 \cdot 5.7\text{SiO}_2$ with $0.4\ \text{ZrO}_2 + 3.2\ \text{TiO}_2$ mol% was melted at Schott AG Mainz. The base glass composition, but with different molar content of zirconia (0.9) and titania (2.2), was previously studied in detail with regard to seed formation [8], [10] and the subsequent crystallisation of the functional Qz-ss [27]. Kleebusch et al. also used the same LAS base glass composition for their TEM analysis of the initial phase separation and subsequent crystallisation of TiO₂ polymorphs, but with 5 mol% TiO₂ and no ZrO₂ [9].

2.2 Thermal analysis

Differential scanning calorimetry (DSC 404 F1 Pegasus, Netzsch, Selb, Germany) was carried out in a lidded PtRh20 at 10 K min⁻¹ with N_2 gas purge to identify the temperature range of the nucleation agent precipitation using a 4.5 × 4.5 mm² platelet (\approx 30 mg) that was prepared from the untreated glass by grinding it to 1 mm thickness.

2.3 Raman Spectroscopy

Changes in the short-range order around the seed former cation Ti^{4+} were studied by Raman spectroscopy (WITec Alpha300, Ulm Germany) during an isothermal treatment (Linkam TS1500 heating stage) at 750, 770, 790, 800 and 820 °C for up to 200 min. An untreated glass platelet was heated at 30 K min⁻¹ to T_x -50 K (with T_x = target temperature), then at 10 K min⁻¹ to T_x -30 K and then at 5 K min⁻¹ to T_x , before Raman spectra (20–3000 cm⁻¹) using a ray shield coupler were recorded (10x objective) every 2 minutes using a frequency-doubled Nd/YAG laser (532 nm) of nominal 25 mW as the incident light source, with a total measurement time of 120 s (6 accumulations with 20 s integration time) and a grating of 600 g mm⁻¹ (1200 cm⁻¹ mean wavenumber).

To visualise the structural changes in their entirety, another platelet was heat-treated in a muffle furnace at 790 °C for 40 min, and Raman analysis was performed at room temperature before and after the heat treatment.

All Raman spectra were background corrected for the intensity at 2000–2500 cm⁻¹ and normalised by setting the remaining total intensity to one. For better comparison and to avoid plots with y-offset, all spectra were normalised in a second step to the main Raman band of the amorphous aluminosilicate network, i.e. to the value at 451 cm⁻¹ [11].

2.4 Kinetic analysis

For the kinetic analysis it was assumed that the first-order phase transition of TiO_2 precipitation obeys the Johnson-Mehl-Avrami-Kolmogorov (JMAK) formalisation, i.e. the time dependence of the volume conversion is described by an S-shaped (sigmoidal) curve for which the following applies:

$$F(t) = 1 - exp\left[-\left(\frac{t}{\tau}\right)^n\right] \tag{1}$$

where F is the converted volume fraction at time t, τ is the characteristic time for the phase transition and n is the Avrami coefficient. The reaction rate is $K = (n/\tau)(t/\tau)^{n-1}$, for n = 1 this results in $K = \tau^{-1}$. Formally, Eq. (1) for n < 1 (n > 1) is identical to a stretched (compressed) exponential function of the Kohlrausch-Williams-Watt (KWW) type and equal to a 2-parameter Weibull distribution function where n is the shape parameter and τ is the scale parameter. All three have in common that an analysis after the transformation of the coordinates $x = \ln(t)$ and $y = \ln(-\ln(1-F))$ is advantageous in order to determine τ and n from the intercept and the slope. Since it is necessary to analyse the decrease in relative intensity R = I(t) / I(t = 0) of the band at 886.3 cm⁻¹ (as shown in the results section), R = 1 - F was set.

This leads to linearisation in the JMAK coordinates:

$$y(x) = n\left(x - \ln(\tau)\right) \tag{2}$$

If a tangent for $x \to 0$ is applied to the data and this slope cannot describe the entire data range as they form a convex function, a second segment must be added after a certain period. A solution to the problem was introduced by Jaing and Murthy [28] for reliability modeling involving two Weibull distributions. In their sectional model, the second Weibull distribution is formulated with three parameters [28]:

$$R_1 = exp\left(-\left(\frac{t}{\tau_1}\right)^{n_1}\right) \tag{3}$$

$$R_2 = exp\left(-\left(\frac{t-\gamma}{\tau_2}\right)^{n_2}\right) \tag{4}$$

where γ is the position parameter, which determines the time at which the second distribution begins. In order to fit Eqs. (3–4) to the data, a transformation into JMAK coordinates was carried out [28]:

$$y(x) = \begin{cases} n_1[x - \ln(\tau_1)], & -\infty < x \le \ln(t_0) \\ n_2[\ln(e^x - \gamma) - \ln(\tau_2)], & \ln(t_0) < x < \infty \end{cases}$$
 (5)

with

$$t_0 = \left[\tau_1^{n_1} \left(\frac{n_2}{n_1} / \tau_2\right)^{n_2}\right]^{\frac{1}{(n_1 - n_2)}} \tag{6}$$

and

$$\gamma = \left(1 - \frac{n_2}{n_1}\right) t_0 \tag{7}$$

which reduces the number of independent parameters from 6 to 4. Eqs. (5–7) demands that $n_1 > n_2$ (convex curve) to ensure $\gamma > 0$ and $t_0 - \gamma > 0$. Jaing and Murthy [28] showed that for $n_1 = n_2$, one obtains $\gamma = 0$ and $\tau_1 = \tau_2$. For this case R(t) reduces to a single Weibull distribution and, thus, $n_1 > n_2$ is required.

The JMAK theory requires a conversion of the entire volume. It is therefore necessary to define a final value of R at which the conversion is complete. For this purpose, the following function was used

$$M = \frac{R_t - R_{\infty}}{R_0 - R_{\infty}} \tag{8}$$

where R_0 , R_t and R_∞ are the relative intensities for zero (0), partial (t), and for the complete (∞) conversion. As the value of R for a complete conversion is not known, two limits were considered here. A lower limit is the assumption that the conversion is completed at R = 0. Eq. (8) is then simplified with $R_\infty = 0$ to $M = R_t / R_0 = R$. An upper limit is obtained by assuming that the conversion is complete at R > 0 and therefore the lowest measured value of R was analysed ($R_\infty = 0.7$ for the band at 886.3 cm⁻¹, see Section 3). It should be noted that the choice of R_∞ only shifts the characteristic times T_1 and T_2 , while the Avrami coefficients n_1 and n_2 remain unchanged.

3. Results

Figure 1 shows that the glass transition (T_g) starts at \approx 670 °C, while the peak of precipitation of the seed former (T_n) is at 810 °C and that of the crystallisation of Qz-ss (T_p) at 854 °C. More precisely, the exothermic signal of the seed former precipitation spans from 745 to 820 °C, which limits the range of isothermal precipitation investigated in subsequent Raman measurements.

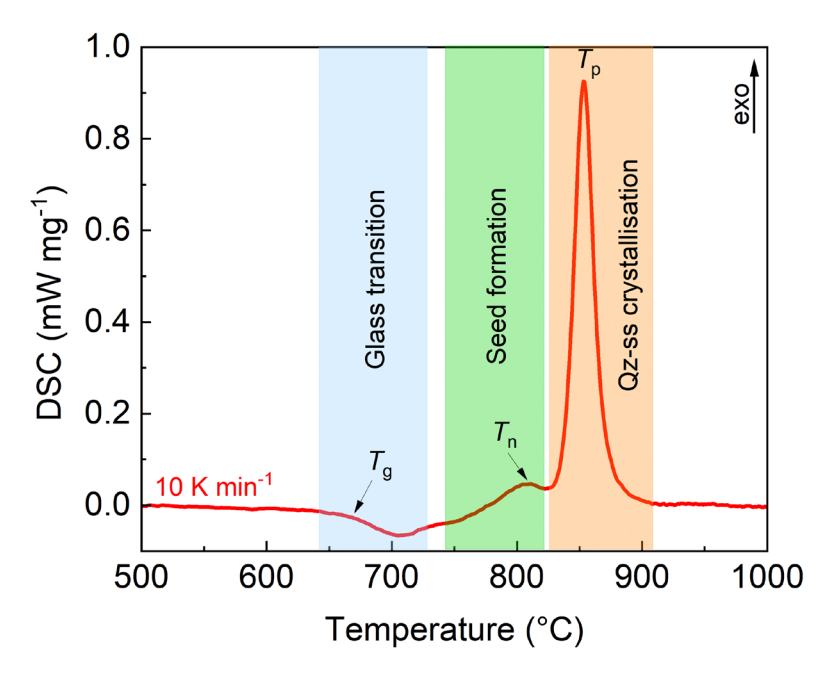


Figure 1. DSC upscan of the untreated LAS glass at 10 K min⁻¹. For clarity, the thermal ranges of the glass transition, seed formation and crystallisation of the quartz solid solution crystals (Qz-ss) are coloured blue, green and orange.

Figure 2 compares the normalised Raman intensity at room temperature before and after a heat treatment at 790 °C for 40 min. The main changes are the decrease of the broad band centred around 900 cm⁻¹ (blue arrow pointing down) and the appearance of a sharp band around 150 cm⁻¹ (blue arrow pointing up). The former is attributed to the loss of Ti⁴⁺ ions (900 cm⁻¹ [11], [26]) and Zr⁴⁺ (950 cm⁻¹ [29]) located in low-coordinated oxygen environments (typically 4- and 5-fold for Ti⁴⁺ and 6-fold for Zr⁴⁺) within the glass network [11], [26], [29], while the latter detects the increase of Ti⁴⁺ (and Zr⁴⁺) in octahedral oxygen coordination within a non-silicate environment, which is associated with the crystallisation of the seed former polymorph(s). Note that bands of Qz-ss are still missing, i.e. in the typical sequence of thermal ceramisation steps of a glass-ceramic production, the sample is 'nucleated' after 40 min at 790 °C (precipitation of the nucleating agent) but not yet 'crystallised' (absence of functional crystals).

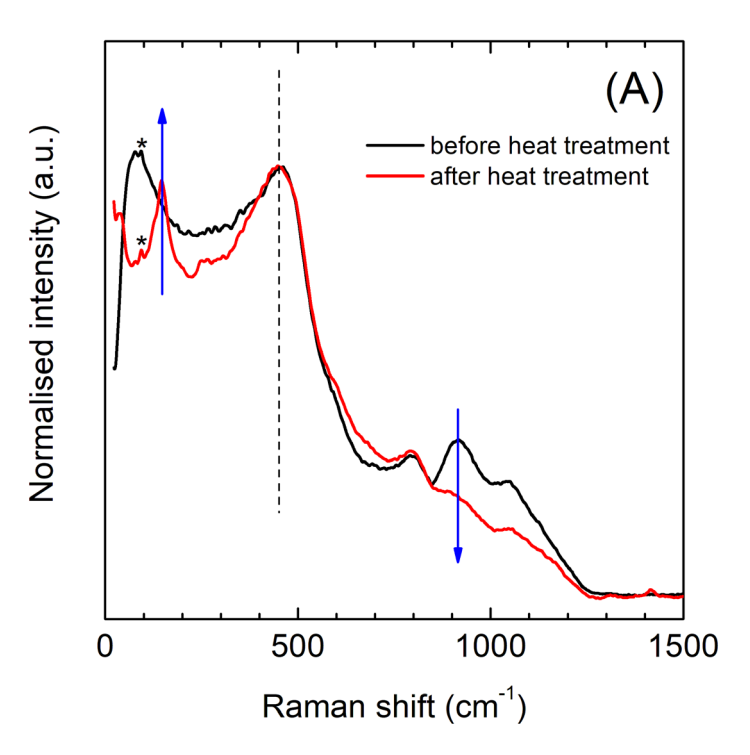


Figure 2. Raman intensity at room temperature of the LAS glass before (black curve) and after (red curve) heat treatment at 790 °C for 40 minutes. The intensity was normalised to the intensity at 451 cm⁻¹ (dashed black line). The blue arrows emphasise the most important changes. The small peak (*) at 95 cm⁻¹ is due to parasitic intensity of the corundum support used.

Figure 3 shows that the state of a nucleated glass was also obtained during isothermal dwelling at 750, 770, 790 and 800 °C (up to 200 min), while the sample at 820 °C already shows the signature of a glass-ceramic, i.e. the crystallisation of the functional Qz-ss with a relatively sharp Raman band at $\approx 465 \text{ cm}^{-1}$ is clear. Note that due to the increasing Qz-ss band, the normalisation of the intensity for this sample at 424.5 cm⁻¹ was performed differently, which led to a crossing point at 825.6 cm⁻¹ as with the other 4 isothermal samples and thus ensured its comparability.

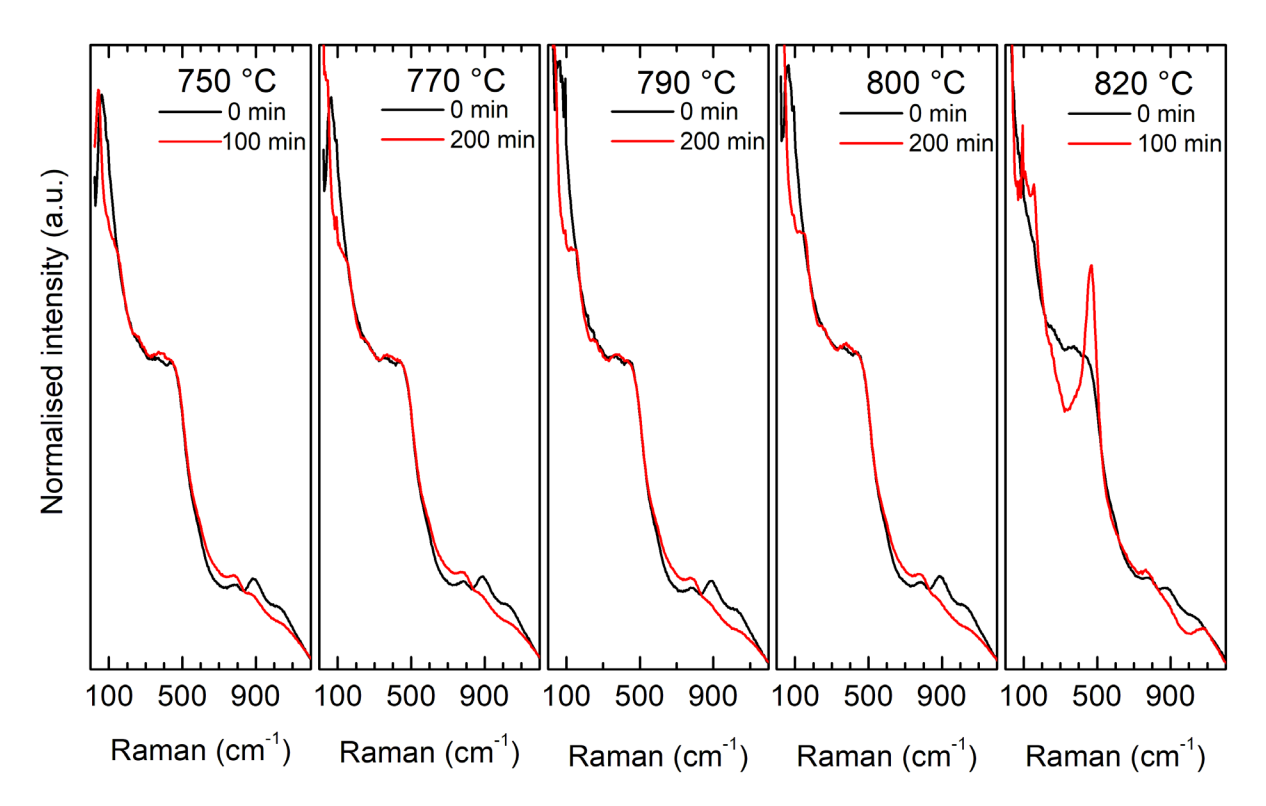


Figure 3. Normalised Raman intensity measured in situ at the start (black line) and end (red line) of an isothermal hold at 750, 770, 790, 800, and 820 °C.

In the following JMAK analysis to determine Avrami coefficients and characteristic times will be based on relative Raman intensities at 886.3 cm⁻¹ and 150–160 cm⁻¹, which were renormalised to the intensity maximum at 451 cm⁻¹ after normalising the spectrum to the total area. Since it is obvious that the effective cross sections of the Raman spectra of glass and crystal are different, normalisation to 451 cm⁻¹ is only applicable if the precipitated crystalline volume is insignificant, so as not to create an artefact through this normalisation. This seems to apply for the nucleated but not yet crystallised glass-ceramics at 750, 770, 790, 800 °C after 100 or 200 min (see Fig. 3) as the total crystal volume is low (up to ~3 vol%). However, after 100 min at 820 °C, this condition no longer appears to apply, resulting in a deviation from the initial intensities near the normalisation frequency at 451 cm⁻¹ and near the crossover frequency 825.6 cm⁻¹.

Figure 4 compares in detail the normalised Raman intensity in the two relevant frequency ranges, which were collected in situ at 800 °C every 2 min up to 200 min in detail. Part (A) shows that TiO₂(B) (≈ 120 cm⁻¹ [26]) together with anatase (≈ 150 cm⁻¹ [26]) are precipitating from the undercooled melt. Since the amount of zirconium cations in the base glass is not negligible and both crystal structures are quite flexible in terms of doping (anatase can incorporate Zr⁴⁺ in up to 7-9 % of the cationic positions [30], [31]), it cannot be ruled out that Zr⁴⁺ will also be incorporated into TiO₂(B) and anatase solid solutions (TiO₂(B)-ss and Ant-ss). The characteristic bands of these two polymorphs appear after approximately 60 min (turquoise curves), while their intensity ratio decreases with time in favour of Ant-ss. Part (B) shows how the band of the lower coordinated Ti⁴⁺ ions in the glass network decreases with time. For the onset of the TiO₂(B)-ss and Ant-ss precipitation, the intensity of the band with the peak at 886.3 cm⁻¹ is already relatively low (turquoise curves) and for longer times it hardly changes. Consequently, the change in coordination appears to occur mainly while the sample is still amorphous, indicating liquid-liquid phase separation on the nanoscale as the initial process. To shed light on this sequence, the relative intensity $R_{886.3} = I_{886.3}(t) / I_{886.3}(t=0)$ was further analysed.

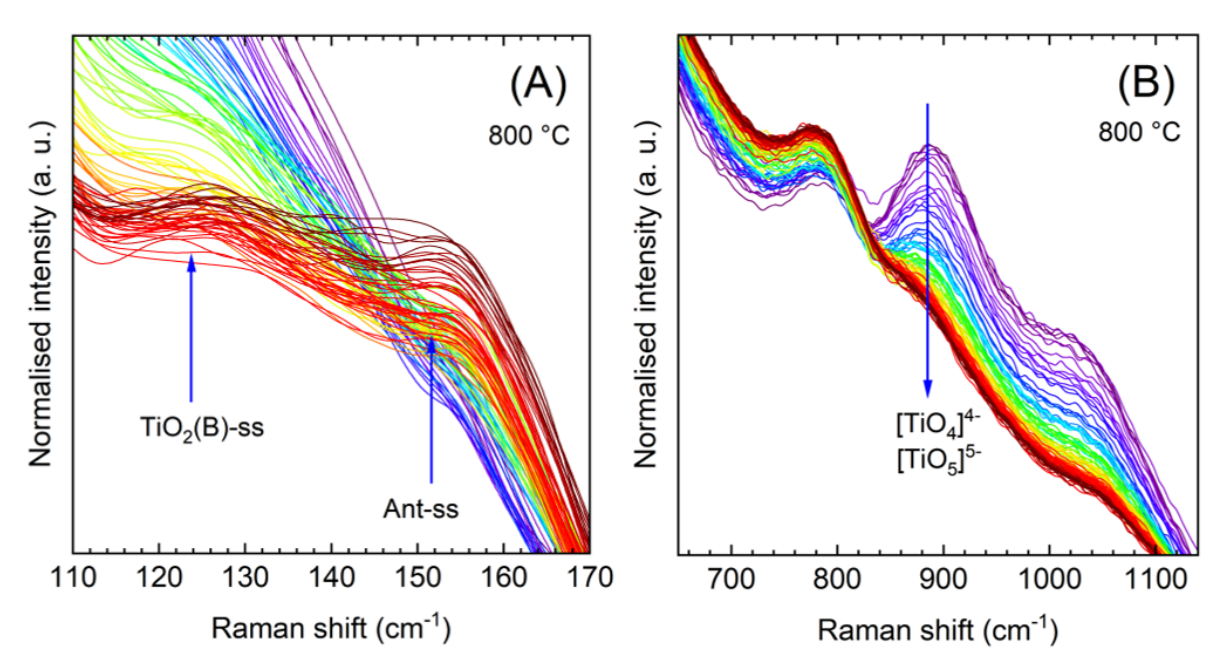


Figure 4. (A) Normalised Raman intensity in the low frequency range (110–170 cm⁻¹) with the characteristic bands of TiO₂(B)-ss and Ant-ss and (B) in the mid frequency range (650–1140 cm⁻¹) at 800 °C. Rainbow colour coding from violet (0 min) to dark red (200 min).

Figure 5 shows $R_{886.3}$ as a function of time. Rainbow colour coding is used to allow a better comparison with the previous spectra. The turquoise coloured dots at about 60 min mark a clear change from a steeper slope of the initial amorphous phase separation to a flatter slope when characteristic bands develop in the low frequency range due to the ordering of the crystalline domains of the polymorphs. The scatter of the data is also larger in the second region. $R_{886.3}$ was transformed into JMAK coordinates to linearise the dependence (see inset of part A). A convex function is obtained, which confirmed that amorphous phase separation and crystal formation are temporally decoupled and the sectional model of Eq. (5) was applied. To determine the kinetic parameters, the tangent R_1 was first fitted to the data for $x \to 0$. A second tangent R_2 for $x \to \infty$ was then applied and the intercept was adjusted so that Eq. (5) matches the data. If $R_\infty = 0.7$ is the upper limit for complete precipitation (resulting in M_1 and M_2 , as illustrated in Eq. (8)), only the ordinate shifts in JMAK coordinates, i.e. the slopes (Avrami coefficients n_1 and n_2) in the two parts remain constant (see part (B) of Figure 5).

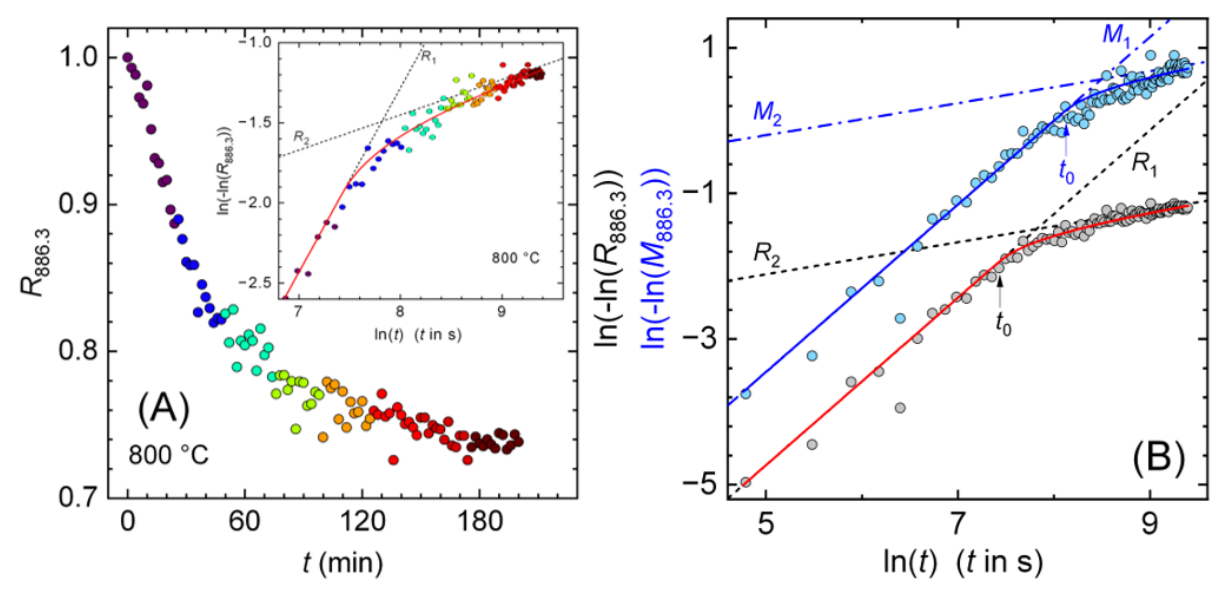


Figure 5. (A) Relative Raman intensity $R_{886.3}$ as a function of time at 800 °C and $In(-In(R_{886.3}))$ versus In(t) (inset) with rainbow colour coding of the data points. Dotted lines are tangents fitted to the data for $x \to 0$ (R_1) and $x \to \infty$ (R_2), while the red line is the fit of Eq. (5) to the full data set. (B) Comparison of the relative Raman intensity in JMAK coordinates for $R_\infty = 0$ (red line) and $R_\infty = 0.7$ (blue line) specifying R_1 , R_2 and M_1 , M_2 as well as t_0 , i.e. the point in time at which the second part becomes effective.

Figure 6 shows analyses for all isothermal heat treatments in this study. The left black ordinate represents the lower limit of R_{∞} , meaning the precipitation is complete at R=0. The right blue ordinate shows the upper limit of R_{∞} , assuming the precipitation is complete at R =0.7. For the latter, the axis is scaled using M values (Eq. 8) while for the former R was kept (as M = R). Both scales clearly show that the processes run faster with increasing temperature, i.e. R_{886.3} (M_{886.3}) becomes smaller for a given value of time. Thus, the characteristic time of first part (related to the amorphous phase separation) decreases from 24709 to 4996 s for $R_{886.3}$ and from 4943 to 1381 s for $M_{886.3}$, which leads to an increase in the conversion rate K. The second part of the process, which is associated with the coordination change during the formation of a crystalline short-range order in the demixed domains, is slower (by 2-3 orders of magnitude) and relatively constant (τ_2 is in the range (2.2–8.8) × 10⁶ s) with exception of the value at 820 K when R_{∞} = 0 is used. Conversely, if R_{∞} = 0.7 is utilised (i.e. $M_{886.3}$), the process appears to be shorter than the first part, with times ranging from 111 to 2980 s (again, except for the value at 820 K). The Avrami coefficients are in the range 0.87-1.15 for the first and 0.17–0.22 for the second stage (Table 1). It can be stated that the characteristic time τ₂ for R_∞ = 0 at 750–800 °C with $(2.2-8.8) \times 10^6$ s (i.e. 25–103 days), is not only significantly longer than the experimentally observed time for the precipitation of the nucleating agent, but also significantly longer than the total time required for the development of the final glass-ceramic microstructure, so that the lower limit ($R_{\infty} = 0$) is therefore no longer taken into account in the following. The exclusion of the lower limit is further supported by the fact that at 820 °C, 100 min (i.e. 1.7 h) was already sufficient to start the latter process (precipitation of Qz-ss), as shown in Fig. 5). Further, it is assumed that the unusual value of τ₂ at 820 °C is influenced by the substantial increase in crystal volume due to the crystallisation of the aluminosilicate matrix, as explained above.

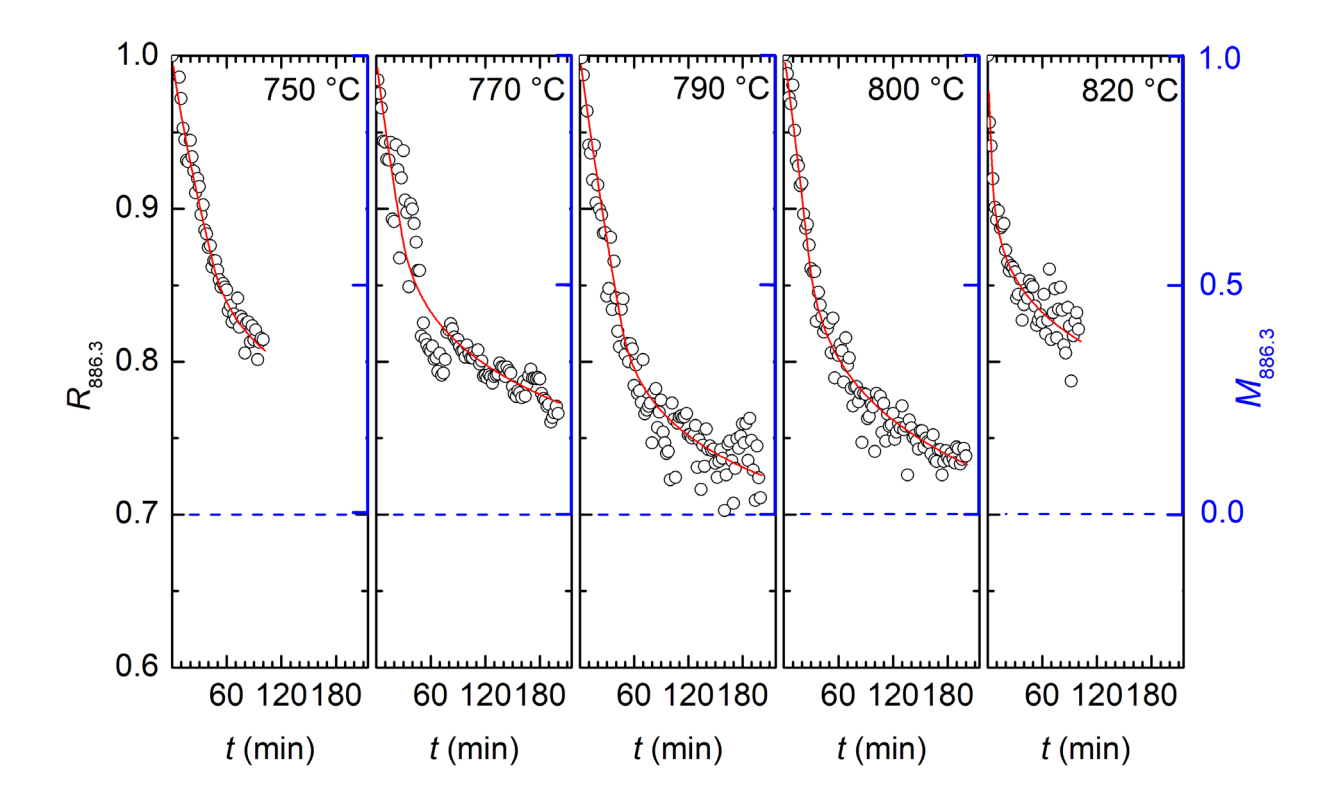


Figure 6. Relative Raman intensities $R_{886.3}$ as a function of time at 750, 770, 790, 800 and 820 °C. The red line is the fit of Eq. (5) to the data using $R_{\infty} = 0$. The right ordinate (blue) is scaled using $M_{886.3}$ values for $R_{\infty} = 0.7$.

Glass sample	750 °	770 °C	790°	800 °C	820 °C
<i>n</i> ₁	0.87	0.92	0.96	1.15	0.91
τ ₁ (s) for <i>R</i> _∞ = 0	24709	16424	15297	9073	4996
τ ₁ (s) for R _∞ = 0.7	4943	3665	3206	2981	1381
n_2	0.2	0.22	0.17	0.22	0.21
τ_2 (s) for $R_{\infty} = 0$	8886111	5150197	7899839	2171457	10750643
t_0 (s) for $R_\infty = 0$	2750	1720	2748	1679	322
T_2 (s) for $R_{\infty} = 0.7$	2980	2269	111	368	7726
t_0 (s) for $R_1 = 0.7$	3707	2718	4559	3306	531

Table 1. Parameters of Eq. (5) used to fit the data.

For the second stage of precipitation, the anatase solid solution (Ant-ss) band at approximately 150 cm⁻¹ was also analysed. Here the tail of the Boson band dominates the Raman intensity at small times, before the formation of the Ant-ss causes an increase in intensity, as Figure 4A shows. As the boson peak belongs to the fraction of the lithium aluminosilicate base glass and here the formation of a crystalline short-range order in the demixed domains is analysed, R_0 in Eq. 8 was set to the lowest value of R. Further, one has to state that at low frequencies Rayleigh scattering, which is sensitive to the demixing process, can superimpose boson peak intensities and thus shift R_0 to longer times, which was also observed: R_0 increased with temperature from 8 min (770 °C) to 10 min (790 °C) and 26 min (800 °C). Hence, characteristic times of the JMAK analysis are probably affected and thus only Avrami coefficients were determined from the increase of the Raman intensities. Furthermore, based on the results of the band at 883.6 cm⁻¹, only the upper limit with the lowest measured value R = 0.93 was taken into consideration for R_{∞} . In addition, F = 1 - R was plotted to account for the increase of

the band and the mean value of the intensity between 150 and 160 cm⁻¹ was analysed in order to enhance the clarity of the signal. Figure 7 shows these data in the JMAK coordinates, whereby for the evaluation only the data $t > t_0$ (Table 1) were taken into consideration due to noisy data and the overlap with the Boson band at short times and therefore only the slope in the second stage was fitted using a single Weibull distribution ($n_1 = n_2$). The analysis showed that in the case of the 750 °C sample, there were only a few data points available as the sample was only recorded up to 100 min ($\ln t < 8.7$ for t in s), while for the other three nucleated glass samples at 770, 790 and 800 °C, slightly higher values than the coefficients given in Table 1 were obtained with $n_2 = 0.34$, 0.33 and 0.3, respectively.

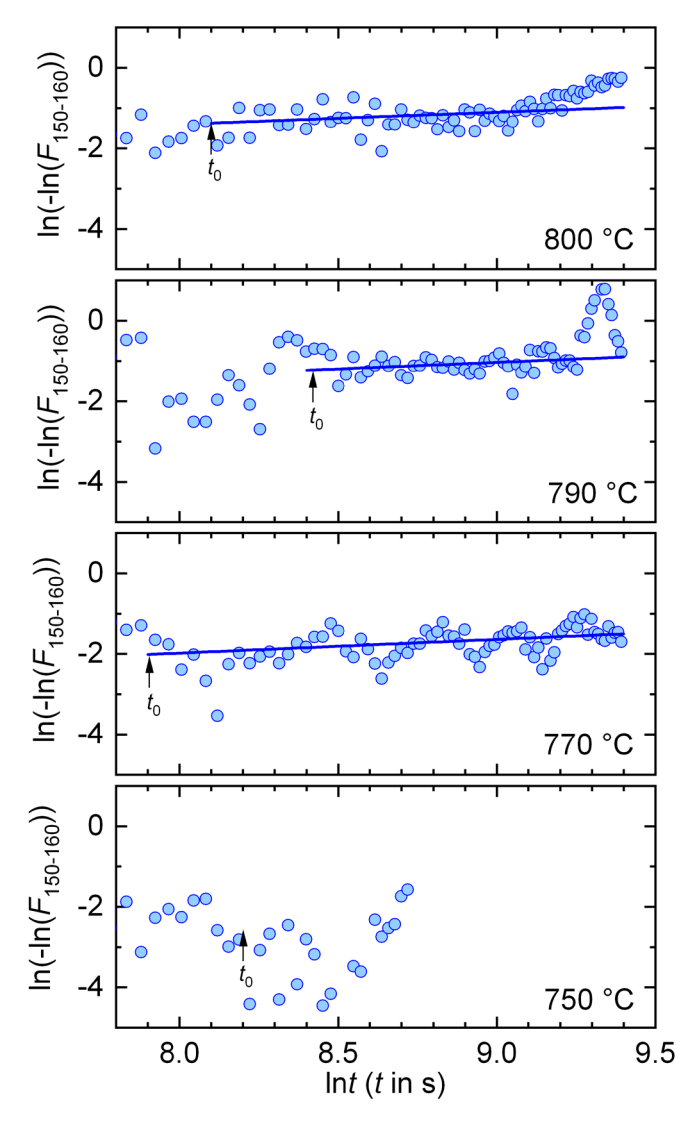


Figure 7. In(-In($F_{150-160}$)) versus In(t) at 750, 770, 790 and 800 °C. The blue line is the fit of Eq. (8) to the data for F_{∞} = 0.07 and t > t₀. Note that F = 1 - R.

For the glass-ceramic sample treated at 820 °C, in which the crystallisation of Qz-ss proceeds simultaneously, as shown in Figure 3, the band of the functional Qz-ss at 465.5 cm⁻¹ was also evaluated in addition to the Ant-ss band at ≈ 150 cm⁻¹. As mentioned above, at 820 °C, the growth of the Qz-ss crystallites and thus the increase in the total crystalline volume fraction above 3% can influence the basis of the JMAK analysis with its normalisation to 451 cm⁻¹, so that the Avrami coefficient was determined solely from the slope of the data of the Qz-ss and Ant-ss bands in JMAK coordinates. Figure 8 shows that higher Avrami coefficients were obtained for this parallel crystallisation at relatively high temperatures. For the nucleating agent n = 0.83, while for Qz-ss a value close to 1.5 was obtained. Furthermore, the division into two

stages no longer appears to be applicable, as t_0 = 531 s (Table 1) was close to the minimum, leaving only three data points for $\ln t_0 < 6.275$.

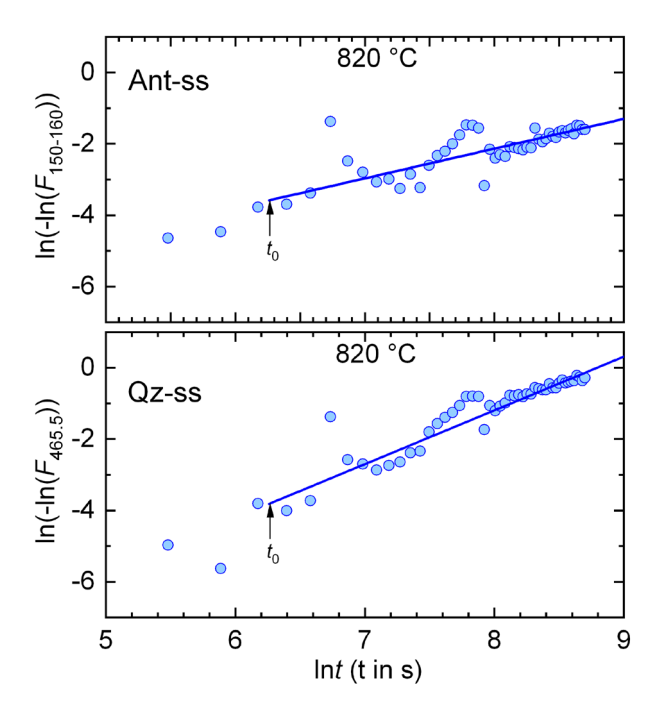


Figure 8. $ln(-ln(F_{150-160}))$ and $ln(-ln(F_{465.5}))$ versus ln(t) at 820 °C. The blue line is the fit of Eq. (8) to the data with $n_1 = n_2$. Only the upper limits for complete precipitation (Ant-ss) and complete crystallisation (Qz-ss) are displayed, with $F_{\infty} = 0.84$ and $F_{\infty} = 0.72$ respectively. Note that F = 1 - R.

4. Discussion

The kinetic analysis of the Raman intensity at 886.3 cm⁻¹ in JMAK coordinates clearly reveals that the process of the seed former precipitation cannot be described by a single mechanism. The coordination changes of Ti⁴⁺ (and possibly Zr⁴⁺) in the amorphous state are much faster $(n \approx 1)$ than during the subsequent formation of a crystalline order within the demixed domains $(n \approx 1/5)$. A lower Avrami coefficient $(n \approx 1/3)$ in the second stage was also confirmed by direct analysis of the Ant-ss band in the 150–160 cm⁻¹ range. Classically, for a diffusion-driven demixing of glass within the metastable immiscibility dome (leading to a binodal microstructure of suspended droplets in a matrix), there is also a two-part division of the kinetic processes, but in the faster first process stage, where chemical supersaturation is removed by steadystate nucleation ($N_v \sim t$, where N_v = volume number density) and growth of the demixed domains with $r \sim t^{1/2}$, one should have n = 2.5, while in the slower second stage, which is associated with the coarsening or ripening of the population of demixed domains $(N_v \sim t^{-1})$, where $r \sim t^{-1}$ $t^{1/3}$), typically $n \approx 0$ [32]. However, these coefficients are obtained when the diffusion field can expand freely around the precipitates (e.g. in the case of a dilute suspension). Smaller coefficients $(r \sim t^{1/6})$ were determined for constrained diffusion, such as for the coarsening of nanosized crystals within a demixed microstructure [33]. At relatively high temperatures (820 °C), the two-stage precipitation of the nucleating agent (Ant-ss) is no longer discernible. The simultaneous precipitation of Qz-ss probably further constrains diffusion pathways, which leads to a decrease in the Avrami coefficient below 1. The faster turnover of melt volume by Qz-ss with n = 3/2 reflects the heterogeneous character of nucleation, in which initially available active sites of the nucleating agent can be utilised. However, it is assumed that the process will slow down significantly with increasing conversion (i.e. with longer times) if these are populated or cannot be supplied quickly enough. It should be noted that n = 3/2 then stands for a diffusive three-dimensional growth on existing precipitates of the nucleating agents as already determined by quantitative high-temperature X-ray diffraction [34]. Furthermore, it becomes clear that the lower Avrami coefficient of the nucleating agent precipitation, in principle, must be taken into account in the practical temperature-time protocol of ceramisation in order to be able to efficiently design the heterogeneous nucleation of Qz-ss.

An earlier TEM study on the precipitation of nucleating agents in this base glass (but with altered Ti to Zr ratio leading to ZrTiO₄ crystallites) determined the size of these crystallites to be around 4 nm [6]. To test whether the coordination change of Ti⁴⁺ leading to the formation of demixed amorphous domains can be controlled by long-range diffusion, the diffusion coefficients D for Ti, Al and O determined in an aluminosilicate glass with albite composition, which is thermally very stable and therefore not affected by crystallisation, were used. It should be noted that among the three types of atoms, aluminium is the least mobile. However, it was recently shown in [35] that, in combination with Ti, the tracer diffusion coefficient of ²⁶Al increases considerably and is almost equal to the diffusivities of ¹⁸O and Ti. For all three, the Arrhenius parameters D_0 = 1.95 × 10⁻⁷ m² s⁻¹ and ΔH_{diff} = 2.68 ± 0.18 eV were determined for the temperature dependence (measuring range of D = 833-900 °C), which suggested a coupled mobility [35]. A structural linkage between AlO₅ and TiO_m (m = 4, 5, 6) polyhedra were expected earlier based on NMR data and RMC modelling in magnesium aluminosilicate glasses [36], [37]. If the time t_{diff} required to diffuse 4 nm is now calculated and set in relation to T₁, the result is 0.02–0.04 for the temperature range under consideration. This means that a diffusion-controlled process can be ruled out (as it takes only 2-4% of the time) and nucleation without growth can be assumed. T1 should then be characteristic of the time associated with the reaction leading to TiO₆ polyhedra and the corresponding structural changes in the linkage with AlO₅ polyhedra. This scenario can be related to the observation of an Al³⁺-enriched shell around TiO₂ solid solutions after their crystallisation [8], [9], [12], [26], which means that purification in the second stage (release of Al3+) is accompanied by the formation of crystalline order in the demixed domains. The total volume transformed is then expected to be negligibly small, which is in agreement with the low Avrami coefficient of ≈ 1/3 determined for the increase of the Ant-ss band in the 150–160 cm⁻¹ range of Figure 7.

In contrast, the Avrami coefficient of the first process stage was in the range of 0.87–1.15, so that $n \approx 1$ and a time-independent rate K can be roughly calculated. For $K_1 = \tau_1^{-1}$, values in the range of $(2.0-7.2) \times 10^{-4} \, \mathrm{s}^{-1}$ are obtained for $R_{\infty} = 0.7$ (Table 1). Since the exact content of crystallisable TiO2 in the glass is not known, an estimate of 3 vol% was made on the basis of the batch composition in order to be able to approximately determine the nucleation rate I_0 in m^{-3} s⁻¹. For a 4 nm demixed domain, which occupies 3 vol%, the volume number density N_v = 8.95×10^{23} m⁻³ will be achieved within the first stage, so that I_0 is in the range of (1.8–6.5) × 10²⁰ m⁻³ s⁻¹. This is in approximate agreement with the nucleation rates of Qz-ss in ZrTiO₄ (up to 1.7 \times 10²¹ m⁻³ s⁻¹ [27]) and ZrSnO₄ (up to 2.7 \times 10¹⁸ m⁻³ s⁻¹ [38]) nucleated LAS glasses. Since the liquid-liquid interfacial energy (≈ 10⁻² J m⁻² [29], [39], [40], [41]) is almost an order of magnitude lower than the crystal-liquid interfacial energy (≈ 10⁻¹ J m⁻² [42], [43], [44]), one would expect much higher nucleation rates in the former case. However, the nucleation of Qzss is heterogeneous (the homogeneous nucleation rate is predicted to be up to 10⁵ m³ s⁻¹ based on the reduced glass transition temperature T_L/T_g (K K⁻¹) = 0.565 [45], [46], with T_L = liquidus temperature ≈ 1390 °C), so that the increase in the nucleation rate by 14 to 15 orders of magnitude is a consequence of the primary precipitation of seed crystallites, which forms a nanostructured environment with interfaces in which different chemical compositions prevail and which considerably reduces the work of critical clustering W* of Qz-ss according to the ideas of the classical nucleation theory ($W^*_{HET} \ll W^*_{HOM}$).

According to non-classical ideas of crystal nucleation, an energetically favourable way is to first achieve a local composition of the phase to be formed and then to build up a crystalline structure [47]. Thus, the generalised Gibbs theory of nucleation already provides for a change in the chemical composition of sub-critical clusters, which overcome the energetic barrier by a change in composition [48], while the 2-step theory initially excludes the growth of sub-critical clusters with the initial composition as density fluctuations and structural fluctuations are separated in time [49]. Irrespective of the exact nature of the clusters as determined by these

theories, the observed temporally decoupled precipitation of TiO₂ polymorphs in LAS glass shows a two-part kinetic process that seems to come close to these ideas.

4. Conclusions

Analysis of the precipitation kinetics using the sectional JMAK equation showed that the overall rate of the faster first stage was almost independent of time, while it was strongly dependent on the heat treatment temperature. The nucleation rate was dominated by a density fluctuation-assisted nucleation mechanism in the amorphous state without any growth, while the second slower stage was governed by structural fluctuations leading to crystalline order in the demixed domains with practically no extra consumption of transformed volume.

Data availability statement

The data presented within this work will be made available on request.

Author contributions

Jessica Streichert: Conceptualisation, Formal analysis, Investigation, Visualisation, Writing – review & editing; Stefanie Meyer: Investigation, Data curation, Visualisation, Validation, Writing – review & editing; Alessio Zandona: Validation, Writing – review & editing; Danilo Di Genova: Validation, Resources, Writing – review & editing; Joachim Deubener: Formal analysis, Supervision, Visualisation, Resources, Writing – original draft.

Competing interests

The authors declare that they have no competing interests.

Acknowledgement

The authors thank Susanne Ibe and Bernd Rüdinger of Schott AG, Mainz, Germany for melting the LAS glass. D. Di Genova acknowledges the funding by Deutsche Forschungsgemeinschaft (DFG) project DI 2751/2-1. J. Deubener acknowledges DFG for funding the project DE598/33-1.

References

- [1] E. D. Zanotto, "A bright future for glass-ceramics", Am. Ceram. Soc. Bul., vol. 89, pp. 19–27, 2010.
- [2] W. Pannhorst, "Overview", in: H. Bach, D. Krause (Ed.), Low Thermal Expansion Glass Ceramics, Springer Berlin Heidelberg, Berlin, Heidelberg, 2005, pp. 1–12. doi: https://doi.org/10.1007/3-540-28245-9 1.
- [3] G. H. Beall, "Design and properties of glass-ceramics", Annu. Rev. Mater. Sci., vol. 22, pp. 91–119, 1992, doi: https://doi.org/10.1146/annurev.ms.22.080192.000515.
- [4] J. Deubener, M. Allix, M. J. Davis, A. Duran, T. Höche, T. Honma, T. Komatsu, S. Krüger, I. Mitra, R. Müller, S. Nakane, M. J. Pascual, J. W. P. Schmelzer, E. D. Zanotto, and S. Zhou, "Updated definition of glass-ceramics", J. Non-Cryst. Solids, vol. 501, pp. 3–10, 2018, doi: https://doi.org/10.1016/j.jnoncrysol.2018.01.033.
- [5] J. Deubener, A. Zandonà, and G. Helsch, "Nomenclature of functional crystals in glass-ceramics: A recommendation based on aluminosilicate solid solutions", J. Non-Cryst. Solids, vol. 633, art-no. 122954, 2024, doi: https://doi.org/10.1016/j.jnon-crysol.2024.122954.

- [6] T. Höche, M. Mäder, S. Bhattacharyya, G. S. Henderson, T. Gemming, R. Wurth, C. Rüssel, and I. Avramov, "ZrTiO₄ crystallisation in nanosized liquid–liquid phase-separation droplets in glass—a quantitative XANES study", Cryst. Eng. Commun., vol. 13, pp. 2550–2556, 2011, doi: https://doi.org/10.1039/C0CE00716A.
- [7] E. Kleebusch, C. Patzig, T. Höche and C. Rüssel, "Effect of the concentrations of nucleating agents ZrO₂ and TiO₂ on the crystallization of Li₂O–Al₂O₃–SiO₂ glass: an X-ray diffraction and TEM investigation, J. Mater. Sci. vol. 51, pp. 10127–10138, 2016, doi: https://doi.org/10.1007/s10853-016-0241-9.
- [8] S. Bhattacharyya, T. Höche, J. R. Jinschek, I. Avramov, R. Wurth, M. Müller, and C. Rüssel, "Direct evidence of Al-Rich layers around nanosized ZrTiO₄ in Glass: Putting the role of nucleation agents in perspective", Crystal Growth & Design., vol. 10, pp. 379–385, 2010, doi: https://doi.org/10.1021/cg9009898.
- [9] E. Kleebusch, C. Patzig, T. Höche, and C. Rüssel, "The evidence of phase separation droplets in the crystallization process of a Li₂O-Al₂O₃-SiO₂ glass with TiO₂ as nucleating agent An X-ray diffraction and (S)TEM-study supported by EDX-analysis", Ceram. Int., vol. 44, pp. 2919–2926, 2018, doi: https://doi.org/10.1016/j.ceramint.2017.11.040.
- [10] R. Donfeu Tchana, T. Pfeiffer, B. Rüdinger, and J. Deubener, "Spectroscopy study on the nucleation kinetics of ZrTiO₄ in a lithium alumosilicate glass", J. Non-Cryst. Solids, vol. 384, pp. 25–31, 2014, doi: https://doi.org/10.1016/j.jnoncrysol.2013.03.006.
- [11] A. Zandonà, A. Scarani, J. Löschmann, M. R. Cicconi, F. Di Fiore, D. de Ligny, J. Deubener, A. Vona, M. Allix, and D. Di Genova, "Non-stoichiometric crystal nucleation in a spodumene glass containing TiO₂ as seed former: effects on the viscosity of the residual melt", J. Non-Cryst. Solids, vol. 619, art-no. 122563, 2023, doi: https://doi.org/10.1016/j.jnoncrysol.2023.122563.
- [12] D. Di Genova, A. Zandonà, and J. Deubener, "Unravelling the effect of nano-heterogeneity on the viscosity of silicate melts: Implications for glass manufacturing and volcanic eruptions", J. Non-Cryst. Solids, vol. 545, art-no. 120248, 2020, doi: https://doi.org/10.1016/j.jnoncrysol.2020.120248.
- [13] D. Di Genova, R. A. Brooker, H. M. Mader, J.W. E. Drewitt, A. Longo, J. Deubener, D. R. Neuville, S. Fanara, O. Shebanova, S. Anzellini, F. Arzilli, E. C. Bamber, L. Hennet, G. La Spina, and N. Miyajima, "In situ observation of nanolite growth in volcanic melt: A driving force for explosive eruptions", Sci. Adv., vol. 6, art-no. abb0413, 2020, doi: https://doi.org/10.1126/sciadv.abb0413.
- [14] A. Scarani, A. Zandonà, F. Di Fiore, P. Valdivia, R. Putra, N. Miyajima, H. Bornhöft, A. Vona, J. Deubener, C. Romano, and D. Di Genova, "A chemical threshold controls nanocrystallization and degassing behaviour in basalt magmas", Comm. Earth Environ., vol. 3, art-no. 284, 2022, doi: https://doi.org/10.1038/s43247-022-00615-2.
- [15] P. Stabile, S. Sicola, G. Giuli, E. Paris, M. R. Carroll, J. Deubener, and D. Di Genova, "The effect of iron and alkali on the nanocrystal-free viscosity of volcanic melts: A combined Raman spectroscopy and DSC study", Chem. Geol., vol. 559, art-no. 119991, 2021, doi: https://doi.org/10.1016/j.chemgeo.2020.119991.
- [16] I. P. Alekseeva, N. M. Belyaevskaya, Ya. S. Bobovich, M. Ya. Tsenter and T. I. Chuvaeva, "Recording, interpretation, and some examples of application of Raman spectra for glass ceramics activated with titanium(IV) oxide", Opt. Spektrosk., vol. 45, pp. 927–936, 1978.
- [17] I. P. Alekseeva, N. M. Belyaevskaya, Ya. S. Bobovich, M. Ya. Tsenter and T. I. Chuvaeva,"An investigation of the crystallization of glasses of the simplest systems activated by TiO₂ and ZrO₂ by means of Raman spectroscopy", Izv. Akad. Nauk SSSR, Neorg. Mater., vol. 16, pp. 732–737, 1980.
- [18] I. P. Alekseeva, N. M. Belyaevskaya, Ya. S. Bobovich, M. Ya.Tsenter, and T. I. Chuvaeva, "A study on the crystallization of glasses activated with TiO₂ and ZrO₂", Izv. Akad. Nauk SSSR, Neorg. Mater., vol. 16, pp. 1587–1592, 1980.
- [19] I. P. Alekseeva, Ya. S. Bobovich, M.Ya. Tsenter, and T. I. Chuvaeva, "Raman spectra of glass ceramics belonging to the Li₂O-Al₂O₃-SiO₂-TiO₂ system and the nature of the phases containing titanium", J. Appl. Spectrosc., vol. 35, pp. 1008–1012, 1981, doi: https://doi.org/10.1007/BF00615796.

- [20] I. P. Alekseeva, Ya. S. Bobovich, M. Ya. Tsenter, and T. I. Chuvaeva, "Spectral features of sitallizing glasses with titanium dioxide," J. Appl. Spectrosc., vol. 36, pp. 215–220, 1982, https://doi.org/10.1007/BF00665177
- [21] I. P. Alekseeva, Ya. S. Bobovich, M. Ya. Tsenter and T. I. Chuvaeva, "Manifestations of the dual nature of titanium in the Raman spectra of lithia-alumina-silica glasses", J. Appl. Spectrosc., vol. 40, pp. 83–88, 1984, doi: https://doi.org/10.1007/BF00661301
- [22] B. Champagnon, A. Boukenter, E. Duval, C. Mai, G. Vigier, E. Rodek, "Early stages of nucleation of Zerodur glass: Very low frequency Raman scattering and small angle Xray scattering investigations", J. Non-Cryst. Solids, vol. 94, pp. 216–221, 1987, doi: https://doi.org/10.1016/S0022-3093(87)80291-0.
- [23] A. A. Zhilin, V. I. Petrov, M. Ya. Tsenter, and T. I., Chuvaeva, "Raman spectroscopy study of the phase decomposition process of lithium aluminosilicate glasses containing TiO₂ and ZrO₂", Opt. Spectrosc., vol. 73, pp. 684–688, 1992.
- [24] R. Sprengard,"Titania-activated nucleation in lithium aluminosilicate glass ceramics investigated by Raman spectroscopy", in: H. Bach and D. Krause (Eds.), Analysis of the structure and composition of glasses and glass ceramics, Springer, Berlin Heidelberg, 1999, pp. 366–379.
- [25] F. Gabel, G. Müller, F. Raether, W. Kiefer, W. Pannhorst, O. Sohr, and R. Sprengard, "Quantitative characterization of nuclei formation by Raman spectroscopy of lithium aluminosilicate glass ceramics doped with titania and zirconia", Phys. Chem. Glasses, vol. 43C, pp. 306–310, 2002.
- [26] A. Zandonà, C. Patzig, B. Rüdinger, O. Hochrein, and J. Deubener, "TiO₂(B) nanocrystals in Ti-doped lithium aluminosilicate glasses", J. Non-Cryst. Solids X, vol. 2, art-no. 100025, 2019, doi: https://doi.org/10.1016/j.nocx.2019.100025.
- [27] M. Dressler, B. Rüdinger, and J. Deubener, "An in-situ high-temperature X-ray diffraction study of early stage crystallization in lithium alumosilicate glass-ceramics", J. Am. Ceram. Soc., vol. 94, pp. 1421–1426, 2011, doi: https://doi.org/10.1111/j.1551-2916.2010.04252.x.
- [28] R. Jiang and D. N. P. Murthy, "Reliability modeling involving two Weibull distributions", Reliab. Eng. Syst. Saf., vol. 47, pp. 187–198, 1995, doi: https://doi.org/10.1016/0951-8320(94)00045-P.
- [29] A. Zandonà, M. Moustrous, C. Genevois, E. Veron, A. Canizares, and M. Allix, "Glass-forming ability and ZrO₂ saturation limits in the magnesium aluminosilicate system", Ceram. Inter., vol. 48, pp. 8433–8439, 2022, doi: https://doi.org/10.1016/j.ceramint.2021.12.051.
- [30] C. Lejon and L. Österlund, "Influence of phonon confinement, surface stress, and zirconium doping on the Raman vibrational properties of anatase TiO₂ nanoparticles", J. Raman Spectrosc., vol. 42, pp. 2026–2035, 2011, doi: https://doi.org/10.1002/jrs.2956.
- [31] D. P. Opra, S. V. Gnedenkov, S. L. Sinebryukhov, E. I. Voit, A. A. Sokolov, E. B. Modin, A. B. Podgorbunsky, Y. V. Sushkov, and V. V. Zheleznov, "Characterization and electrochemical properties of nanostructured Zr-doped anatase TiO₂ tubes synthesized by solgel template route", J. Mater. Sci. Technol., vol. 33, pp. 527–534, 2017, doi: http://dx.doi.org/10.1016/j.jmst.2016.11.011.
- [32] J. Deubener, Z. A. Osborne, and M. C. Weinberg, "Determination of the liquid-liquid surface energy in phase separating glasses", J. Non-Cryst. Solids, vol. 215, pp. 252–261, 1997, doi: https://doi.org/10.1016/S0022-3093(97)00089-6.
- [33] J. O. Fritzsche, B. Rüdinger, and J. Deubener, "Slow coarsening of tetragonal zirconia nanocrystals in a phase-separated sodium borosilicate glass", J. Non-Cryst. Solids, vol. 606, art-no. 122206, 2023, doi: https://doi.org/10.1016/j.jnoncrysol.2023.122206.
- [34] A. Zandonà, B. Rüdinger, and J. Deubener, "A threshold heating rate for single-stage heat treatments in glass-ceramics containing seed formers", J. Am. Ceram. Soc., vol. 104, pp. 4433–4444, 2021, doi: https://doi.org/10.1111/jace.17822.
- [35] P. Fielitz, G. Helsch, G. Borchardt, and J. Deubener, "Al-26 and O-18 tracer diffusion in a titania-coated sodium aluminosilicate glass", J. Non-Cryst. Solids, vol. 614, art-no. 122400, 2023, doi: https://doi.org/10.1016/j.jnoncrysol.2023.122400.

- [36] M. Guignard, L. Cormier, V. Montouillout, N. Menguy, D. Massiot, and A. C. Hannon, "Environment of titanium and aluminum in a magnesium aluminosilicate glass", J. Phys. Condens. Matter, vol. 21, art-no. 375107, 2009, doi: https://doi.org/10.1088/0953-8984/21/37/375107.
- [37] M. Guignard, L. Cormier, V. Montouillout, N. Menguy, and D. Massiot, "Structural fluctuations and role of Ti as nucleating agent in an aluminosilicate glass", J. Non. Cryst. Solids, vol. 356, pp. 1368–1373, 2010, doi: https://doi.org/10.1016/j.jnoncrysol.2010.04.004.
- [38] M. Dressler, B. Rüdinger, and J. Deubener, "Crystallization kinetics in a lithium alumosilicate glass using SnO₂ and ZrO₂ additives, J. Non-Cryst. Solids, vol. 389, pp. 60–65, 2014,doi: https://doi.org/10.1016/j.jnoncrysol.2014.02.008.
- [39] L. Wondraczek, J. Deubener, H. del Pozo, and A. Habeck, "Interfacial energy in phase-separated glasses from emulsion rheology", J. Am. Ceram. Soc., vol. 88, pp. 1673–1675, 2005, doi: https://doi.org/10.1111/j.1551-2916.2005.00325.x.
- [40] A. Dittmar, H. Bornhöft, and J. Deubener, "Coarsening kinetics in demixed lead borate melts", J. Chem. Phys., vol. 138, art-no. 224502, 2013, doi: https://doi.org/10.1063/1.4808162.
- [41] D. Bouttes, O. Lambert, C. Claireaux, W. Woelffel, D. Dalmas, E. Gouillart, P. Lhuissier, L. Salvo, E. Boller, and D. Vandembroucq, "Hydrodynamic coarsening in phase-separated silicate melts", Acta Mater.,vol. 92, pp. 233–242, 2015, doi: https://doi.org/10.1016/j.actamat.2015.03.045.
- [42] P. F. James, "Kinetics of crystal nucleation in silicate glasses", J. Non-Cryst. Solids, vol. 73, pp. 517–540, 1985, doi: https://doi.org/10.1016/0022-3093(85)90372-2.
- [43] J. Deubener and M. C. Weinberg, Crystal-liquid surface energies from transient nucleation, J. Non-Cryst. Solids, vol. 231, pp. 143–151, 1998, doi: https://doi.org/10.1016/S0022-3093(98)00412-8.
- [44] V. M. Fokin, E. D. Zanotto, N. S. Yuritsyn, and J. W. P. Schmelzer, "Homogeneous crystal nucleation in silicate glasses: A 40 years perspective", J. Non-Cryst. Solids, vol. 352, pp. 2681–2714, 2006, doi: https://doi.org/10.1016/j.jnoncrysol.2006.02.074.
- [45] J. Deubener, "Compositional onset of homogeneous nucleation in (Na, Li) disilicate glasses", J. Non-Cryst. Solids, vol. 274, pp. 195–201, 2001 doi: https://doi.org/10.1016/S0022-3093(00)00188-5.
- [46] V. M. Fokin, E. D. Zanotto, and J. W. P. Schmelzer, "Homogeneous nucleation versus glass transition temperature of silicate glasses", J. Non-Cryst. Solids, vol. 321, pp. 52–65, 2003, doi: https://doi.org/10.1016/S0022-3093(03)00089-9.
- [47] L. Cormier, "Nucleation in glasses new experimental findings and recent theories, Proc. Mater. Sci., vol. 7, pp. 60–71, 2014, doi: https://doi.org/10.1016/j.mspro.2014.10.009.
- [48] P. G. Vekilov, "Dense liquid precursor for the nucleation of ordered solid phases from solution", Cryst. Growth Des., vol. 4, pp. 671-685, 2004, doi: https://doi.org/10.1021/cg049977w.
- [49] J. W. P. Schmelzer, G. S. Boltachev, and V. G. Baidakov, "Classical and generalized Gibbs' approaches and the work of critical cluster formation in nucleation theory. J. Chem. Phys., vol. 124, art-no. 194503, 2006, doi: https://doi.org/10.1063/1.2196412.